Efficient radially polarized laser beam generation with a double interferometer

Steve C. Tidwell, Gerald H. Kim, and Wayne D. Kimura

Conversion of a linearly polarized CO_2 laser beam into a radially polarized beam is demonstrated with a novel double-interferometer system. The first Mach–Zehnder interferometer converts the linearly polarized input beam into two beams with $\sin^2\theta$ and $\cos^2\theta$ intensity profiles, where θ is the azimuthal angle. This is accomplished by using two spiral-phase-delay plates with opposite handedness in the two legs of the interferometer to impart a one-wave phase delay azimuthally across the face of the beams. After these beams are interfered with, the resulting beams are sent directly into the second Mach–Zehnder interferometer, where the polarization direction of one beam is rotated by 90°. The beams are then recombined at the output of the second interferometer with a polarization-sensitive beam splitter to generate a radially polarized beam. The output beam is ≈92% radially polarized and contains ≈85% of the input power. This system will be used in upcoming laser particle acceleration experiments.

Key words: Radial polarization, double interferometer, spiral-phase-delay plate, laser particle acceleration.

1. Introduction

In a previous paper[1] we demonstrated that a radially polarized laser beam can be created by interfering with two linearly polarized beams with tailored intensity and phase profiles. An argon ion laser lasing at 0.5145 μm was used for this demonstration. Although our technique worked well and demonstrated the underlying principles, it did not use the most convenient and optimal method for our particular application. This application is laser particle acceleration experiments, where we will be using a high peak power CO_2 laser to accelerate relativistic electrons to high energies by use of the inverse Cerenkov interaction.[2,3] The laser wavelength in this case is in the infrared ($\lambda \sim 10$ μm), and the beam has a linearly polarized TEM_{00} Gaussian profile.

Two methods for generating a radially polarized beam from a linearly polarized beam were presented in Ref. 1. The first requires the laser to operate in a linearly polarized TEM_{01} Gaussian mode. This beam is split into two equal components, one component is rotated by 90°, and the beams are recombined with the proper phase to create a radially polarized beam. This method converts linear polarization into radial polarization efficiently but requires a TEM_{01} mode output from the laser, and the method is sensitive to nonsymmetric azimuthal intensity variations in the input beam profile.

The second method creates a radially polarized beam by combining two circular-polarized laser beams with opposite handedness. Each circularly polarized beam has an azimuthally varying phase delay that is one wave deep. This unusual phase delay is produced with a spiral-phase-delay plate, which will be described in more detail in Section 3. This second method is less sensitive to input field variations, but the maximum conversion efficiency to radially polarized light is <50%.

The method presented in this paper is a hybrid of the earlier two approaches. The result is a system that is able to accept any linearly polarized laser beam profile and convert it to radial polarization with high efficiency. This particular system is also designed to operate in the infrared. Section 2 reviews the theory associated with this hybrid system. Section 3 describes the experimental optical system. The experimental results are presented in Section 4, and a discussion is given in Section 5. Section 6 ends the paper with a summary.

2. Theory

As shown in Ref. 1, a radially polarized laser beam can be created by coherently combining two beams, one with an intensity distribution following a $\sin^2\theta$

The authors are with STI Optronics, Inc., 2755 Northup Way, Bellevue, Washington 98004-1495.

Received 13 October 1992.
0003-6935/93/275222-08$06.00/0.

dependence and the other with a $\cos^2\theta$ dependence, where θ is the azimuthal angle. This is shown schematically in Fig. 1. This in fact is the basis of the first method described in Ref. 1, in which TEM_{01} and TEM_{10} laser beams are used. We show in this section that it is possible to create the $\sin^2\theta$ and $\cos^2\theta$ laser beams from a linearly beam with an arbitrary intensity profile. Once this is accomplished, a radially polarized laser beam is made by use of the same basic technique as the first method in Ref. 1. As explained in Sec. 3, this whole process is achieved by using two Mach–Zehnder interferometers positioned back to back in a double-interferometer configuration. The first interferometer converts the linearly polarized laser beam into $\sin^2\theta$ and $\cos^2\theta$ intensity distributions; the second interferometer combines the $\sin^2\theta$ and $\cos^2\theta$ beams to make a radially polarized laser beam. The following is a simplified analysis; a more comprehensive analysis is given in the Appendix.

Assume we wish to coherently mix two linearly polarized laser beams, E_1 and E_2, each of which has a phase variation that is a function of θ, with the phase variations equal but opposite. The expressions for these two beams are

$$E_1 = \frac{E_0}{\sqrt{2}} \exp[-if(\theta)], \tag{1}$$

$$E_2 = \frac{E_0}{\sqrt{2}} \exp[if(\theta)], \tag{2}$$

where E_0 is a constant and the radial and temporal dependences have been ignored. These two beams are combined at some dielectric interface (e.g., a beam splitter) as shown in Fig. 2, where the indices of refraction of the media are given by n_1 and n_2 and $n_2 > n_1$. The resultant beams, E_3 and E_4, consist of the reflected and transmitted components of E_1 and E_2 such that

$$E_3 = E_{1_r} + E_{2_t}, \tag{3}$$

$$E_4 = E_{1_t} + E_{2_r}, \tag{4}$$

where the r and t subscripts refer to the reflected and transmitted components, respectively; we assume they are equal in magnitude (i.e., we are using a 50/50 beam splitter). From Eqs. (1) and (2), and recalling that reflection off a medium with higher index results in a π phase shift, these components are

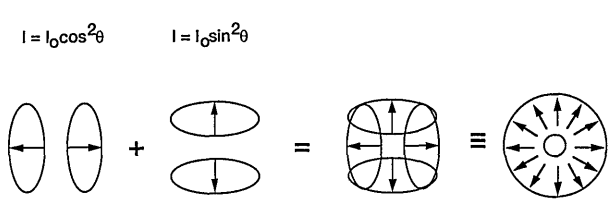

Fig. 1. Coherent combination of laser beams with $\cos^2\theta$ and $\sin^2\theta$ intensity distributions yields a radially polarized beam.

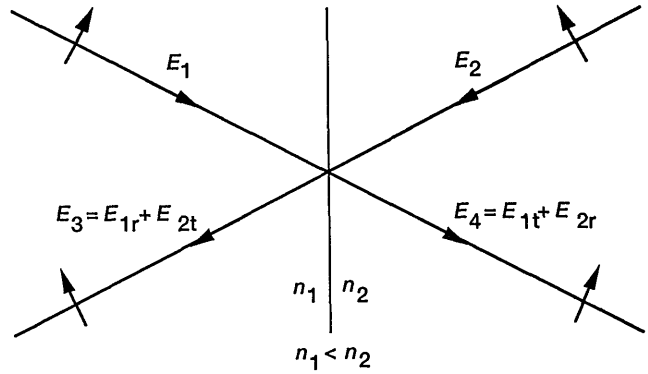

Fig. 2. Configuration for combining beams E_1 and E_2 at dielectric boundary with indices of refraction n_1 and n_2, where $n_2 > n_1$.

given by

$$E_{1_r} = \frac{E_1}{\sqrt{2}} \exp(i\pi) = \frac{-E_0}{2} \exp[-if(\theta)], \tag{5}$$

$$E_{1_t} = \frac{E_1}{\sqrt{2}} = \frac{E_0}{2} \exp[-if(\theta)], \tag{6}$$

$$E_{2_r} = \frac{E_2}{\sqrt{2}} = \frac{E_0}{2} \exp[if(\theta)], \tag{7}$$

$$E_{2_t} = \frac{E_2}{\sqrt{2}} = \frac{E_0}{2} \exp[if(\theta)]. \tag{8}$$

The intensity profile of the E_3 beam is then

$$\begin{aligned} I_3 &= E_3 \times E_3^* = (E_{1_r} + E_{2_t})(E_{1_r}^* + E_{2_t}^*) \\ &= (E_{1_r}E_{1_r}^* + E_{2_t}E_{2_t}^* + E_{1_r}E_{2_t}^* + E_{2_t}E_{1_r}^*) \\ &= E_0^2\{2 - \exp[-2if(\theta)] - \exp[2if(\theta)]\}/4. \end{aligned} \tag{9}$$

But $\sin^2\gamma = [2 - \exp(-2i\gamma) - \exp(2i\gamma)]/4$, so that

$$I_3 = I_0 \sin^2[f(\theta)], \tag{10}$$

where $I_0 \equiv E_0^2$. Because we want $I_3 = I_0 \sin^2\theta$, this implies that $f(\theta) = \theta$. This means the phase delay needed on E_1 and E_2 is simply equal to the azimuth angle or, equivalently, what is referred to as a spiral phase delay. Using the same analysis as above, we can show that $I_4 = I_0 \cos^2\theta$. Hence two oppositely handed spiral-phase-delay plates can be used in the first interferometer to convert linearly polarized light into $\sin^2\theta$ and $\cos^2\theta$ intensity distributions.

3. Description of Radial-Polarization Converter Optical System

A. Double-Interferometer System

Figure 3 depicts a schematic view of the radial polarization converter double-interferometer system. The linearly polarized input beam enters the first interferometer through a 50/50 beam splitter. The transmitted and reflected beams travel through right-

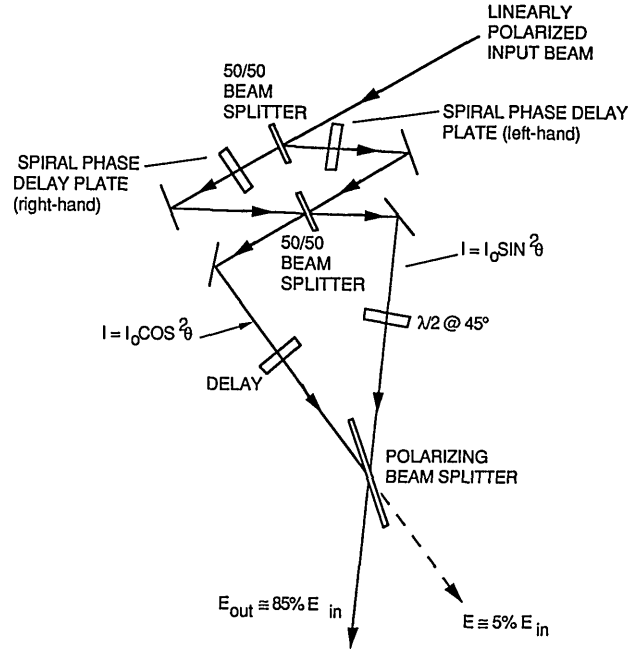

Fig. 3. Schematic layout of the radial-polarization converter optical system.

and left-handed spiral-phase-delay plates, respectively. These beams are then recombined at the second 50/50 beam splitter, which is also the entrance optic to the second interferometer. The transmitted and reflected beams now have $\sin^2\theta$ and $\cos^2\theta$ intensity distributions. Note that the angles of incidence in this portion of the radial-polarization converter are kept as small as possible ($\lesssim 10°$) to avoid angle-dependent variations in the transmission and reflection of the beam splitters.

Before we combine the $\sin^2\theta$ and $\cos^2\theta$ beams to create a radially polarized beam as illustrated in Fig. 1, the polarization of the $\cos^2\theta$ beam must be rotated by 90°. This is because the first interferometer only changes the intensity distribution; it does not affect the polarization direction of the linearly polarized input beam. This polarization rotation is achieved by using a CdS half-wave ($\lambda/2$) plate oriented at 45° to the input beam polarization direction. The gross phase delay caused by the half-wave plate is compensated for by using an antireflection-coated ZnSe substrate of equal thickness in the opposite leg of the second interferometer. It is important that the opposing interferometer legs be approximately equal in length because the input pulse length from the CO_2 laser is only ~10 ps or ~3 mm in our application.

To maximize the conversion efficiency, a ZnSe polarization-sensitive (Brewster's angle) beam splitter is used at the output of the second interferometer to combine the $\sin^2\theta$ and $\cos^2\theta$ beams. In principle, this should convert $\approx 85\%$ of the energy in the $\sin^2\theta$ and $\cos^2\theta$ beams into one radially polarized beam rather than $<50\%$ as in the earlier design.[1]

B. Spiral-Phase-Delay Plate

A sketch of the spiral-phase-delay plate appears in Fig. 4. It consists of a ZnSe coating deposited onto a ZnSe substrate in which the coating thickness increases uniformly in a spiral around the substrate surface. At its thickest point, the coating is one wave thick ($\lambda = 10.2$ μm) and corresponds to a physical thickness of 6.3 μm. The plate was coated by Reynard Enterprises, San Clemente, Calif.[4]

The coating and substrate materials are kept the same to help avoid stress in the coating and reflection at the coating–substrate boundary. Nevertheless cw CO_2 laser interferometer tests together with HeNe laser Fizeau measurements of the plate indicate that the index of refraction of the coating is 2.6 at $\lambda = 10.2$ μm, which is roughly 8% higher than typical quoted values for bulk ZnSe.

A self-interference pattern of the coating at 632.8 nm is shown in Fig. 5, revealing a spoke-like pattern caused by the ramp of the coating. The uniform spacing of the fringes and their straightness indicate that the slope of the ramp is approximately constant in the azimuthal direction and zero in the radial direction. The only notable fabrication problem is that the fringes do not radiate from a common point. This difficulty will degrade the performance of the converter somewhat. The step in the coating where the top of the ramp meets the bottom can also be clearly seen.

C. Laser Acceleration Optical System

To better understand the data that will be presented regarding the radial-polarization converter, it is helpful to explain the optical system in which it is being used. Figure 6 is a schematic view of the optical system for the laser acceleration experiments.[2] The experiment is located in the Accelerator Test Facility (ATF) at Brookhaven National Laboratory and uses the ATF high peak power (10–100 ps) CO_2 laser. This laser beam enters the optical system as shown in the upper right-hand corner of Fig. 6. The other lasers depicted in Fig. 6 are used to align the optical system. The laser beam entering the radial polarization converter is 2 cm in diameter.

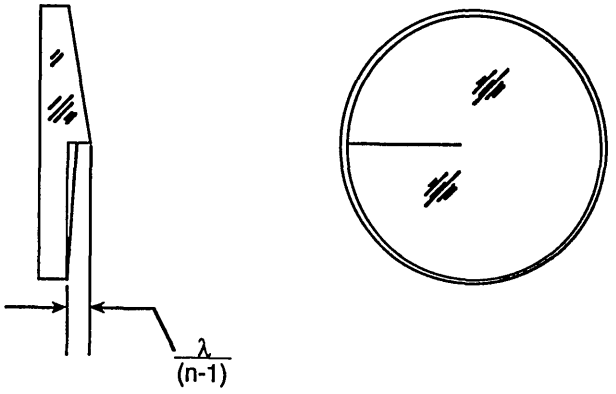

Fig. 4. Sketch of the spiral-phase-delay plate. The coating thickness has been greatly exaggerated for clarity.

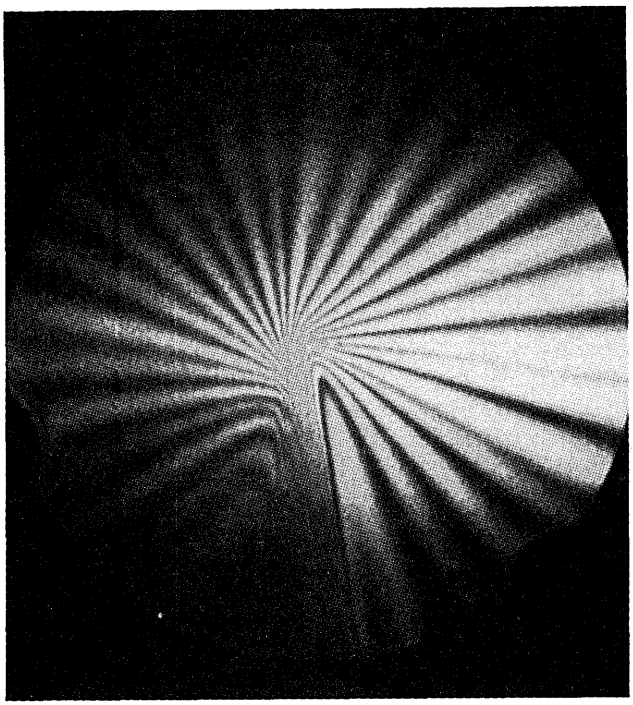

Fig. 5. Self-interference fringe pattern of the spiral-phase-delay plate coating taken with a HeNe laser (λ = 632.8 nm).

The lower left-hand corner of Fig. 6 shows the gas cell where the laser acceleration process occurs. (In inverse Čerenkov, a gas is used to slow the velocity of the light to match the electron velocity.) The radially polarized laser beam is focused onto the electron beam by use of an axicon mirror with a small hole in its center through which the electron beam travels. Between the radial-polarization converter and the gas cell are optics for reducing the beam diameter to 1 cm and for relaying imaging of the radially polarized beam onto the axicon mirror. This latter point is important because the laser beam exiting the converter contains diffraction effects caused primarily by the step in the spiral-phase-delay plate coating (see Fig. 5). By relaying imaging from the spiral-phase-delay plates to the axicon, these diffraction effects can be minimized.

4. Experimental Results

When the radially polarized beam is focused by the axicon mirror, the resultant transverse intensity distribution follows a $J_1(r)$ pattern, where J_1 is the Bessel function of the first kind of order one and r is the radial position.[5,6] An idealized computer-generated $J_1(r)$ intensity profile (negative image) is given in Fig. 7(a), where the beam parameters have been selected to facilitate comparison with the experimen-

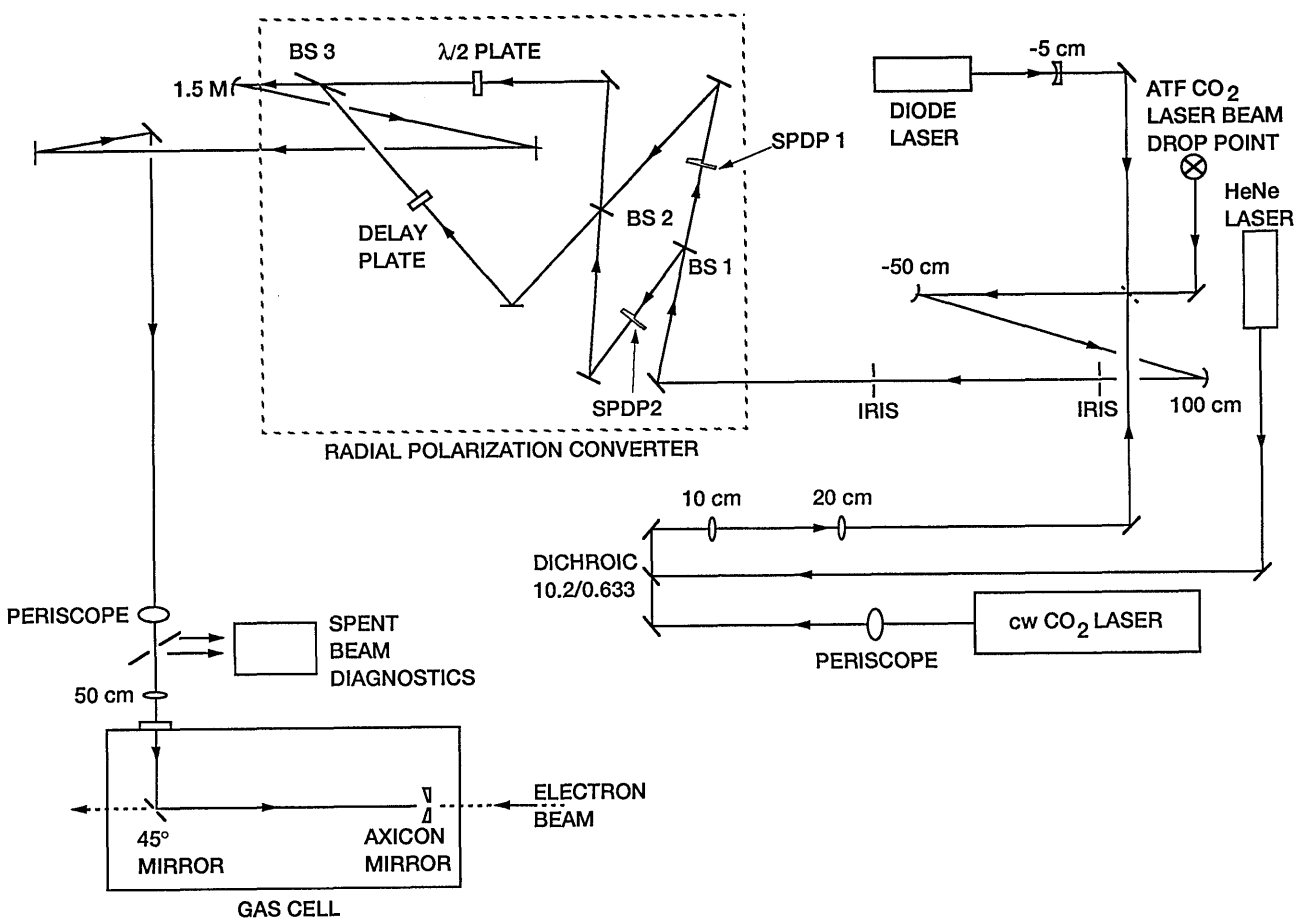

Fig. 6. Schematic of the inverse Čerenkov laser acceleration experiment optical system showing the location of the radial-polarization converter system. BS, beam splitter.

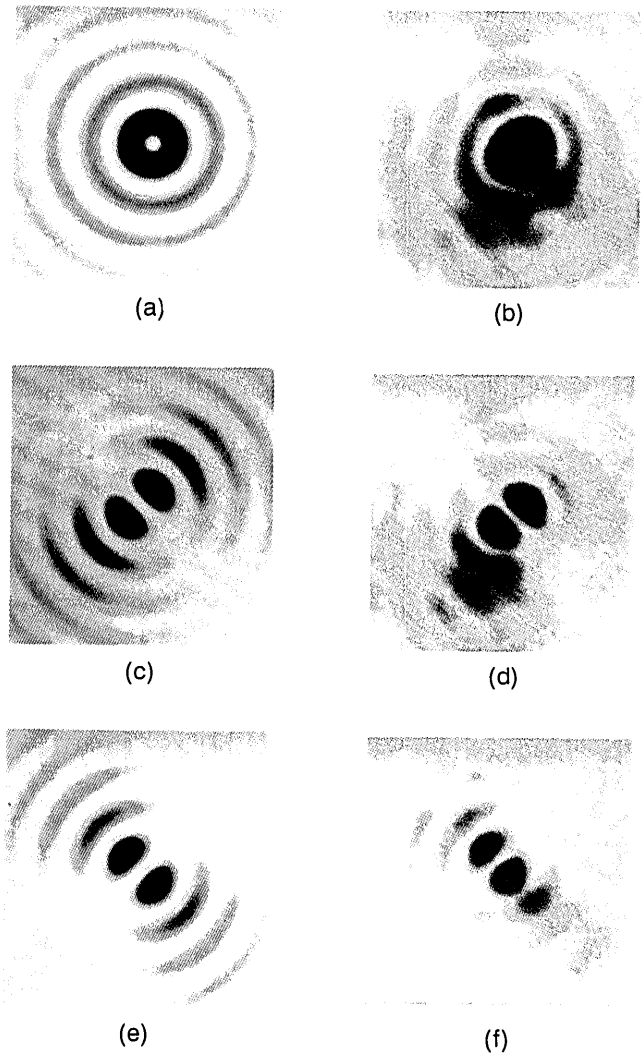

Fig. 7. CO_2 laser beam intensity profile within the axicon focal region inside the gas cell (see Fig. 6). Full profile of the radially polarized laser beam showing a $J_1(r)$ Bessel pattern distribution: (a) theoretical prediction; (b) experimentally measured distribution using the cw CO_2 alignment laser (see Fig. 6). Resultant profile after transmission through a linear polarizer oriented at 45° (i.e., perpendicular to the null in the center of the pattern): (c) theoretical prediction; (d) experimentally measured distribution. Resultant profile after transmission through a linear polarizer oriented at 135°: (e) theoretical prediction; (f) experimentally measured distribution.

tal data. The experimental $J_1(r)$ intensity pattern is measured by imaging the axicon-focused beam onto an infrared-sensitive video camera and is shown in Fig. 7(b). These data are taken using the cw CO_2 laser (see Fig. 6). Note that both patterns have a distinct null in the center, which is unlike the usual Airy pattern created by diffraction around a circular aperture.

To verify that the axicon-focused beam is radially polarized, the beam is sent through a linear polarizer (analyzer), which can be rotated. The transmitted intensity pattern should appear like that shown in Fig. 7(c), which is the case for the idealized Bessel beam. In Fig. 7(c) the analyzer is oriented with its transmission axis perpendicular to the null through the center of the pattern. If the analyzer is rotated in θ, this pattern will also rotate. An example of this for the idealized Bessel beam case is given in Fig. 7(e), which shows the pattern when the analyzer is rotated by 90° with respect to its orientation in Fig. 7(c).

A wire grid polarizer is used to analyze the experimentally obtained Bessel beam in Fig. 7(b). The results are shown in Figs. 7(d) and 7(f) for the same azimuthal angle orientations as the idealized cases depicted in Figs. 7(c) and 7(e), respectively. We see that there is good agreement with theory. The analyzer orientation angle for these measurements is intentionally chosen to be 45° and 135° relative to the orientation of the $\sin^2\theta$ and $\cos^2\theta$ beams (cf. Fig. 1). This represents a worst-case test because although the direction of polarization along the principle axes of the beam does not require interference in the second interferometer, the polarization along the diagonals depends entirely on interference.

Because the profiles in Figs. 7(d) and 7(f) also constitute an orthogonal polarization set, they also contain all the information necessary to determine the purity of the radially polarized beam. The vector sum of the field at a point in one of the profiles with the corresponding point in the other profile indicates the direction of the beam polarization relative to the center of the beam. If the beam is perfectly radially polarized, the vector sum of these polarization components will yield a net field vector oriented along the radius of a circle with a center that is the center of the beam. If the beam is not perfectly radially polarized, then the net field vector will not be exactly along a radius. Relative to the ideal radial direction, this net field vector can be decomposed into its radial and azimuthal components. (This calculation assumes the wave fronts are flat for both profiles.) The sum of all the radial components divided by the total amount of light in both polarization images then gives the radial-polarization purity of the laser beam.

One limitation when analyzing digitized video images is that the dynamic range for each pixel is only 0 to 255 (8-bit depth). Images that are less than 1 in magnitude are truncated to 0 value. This means that even the ideal case will not yield 100% radial polarization. Instead the idealized case [Figs. 7(c) and 7(e)] has a radial-polarization purity of only 99.93%. The data [Figs. 7(d) and 7(f)] have a calculated radial-polarization purity of $\approx 92\%$. This value of radial-polarization purity is also obtained when performing the same analysis on the beam before it is focused by the axicon.

5. Discussion

The less than perfect radial-polarization purity is probably a result of errors in the spiral-phase-delay plates. For example, as seen in Fig. 5, the fringes do not radiate from a common point in the center of the plate. This implies some variation away from the radial direction and, therefore, the existence of some azimuthal polarization components. The video anal-

ysis program also indicates that azimuthal polarization components are concentrated along the diagonal (i.e., 45°) axes. As mentioned earlier, this is the area that is most sensitive to imperfect interference between the beams.

To be useful, all the optical elements of the radial-polarization converter system must be able to tolerate the expected laser fluence during the experiment. The weakest element of the system with regard to optical damage is the spiral-phase-delay plate coating. Laser-damage tests were performed on a sample spiral-phase-delay coating with the ATF CO_2 laser ($\lambda = 10.6\ \mu m$). The laser beam is focused onto various locations on the coating including the step region. No laser damage is observed at fluences up to at least 190 mJ/cm^2 at a pulse length of 100 ps (1.9 GW/cm^2). This is above the maximum fluence expected from the ATF laser during the experiment.

6. Summary

A double-interferometer system for converting a linearly polarized laser beam to a radially polarized one has been demonstrated. Unlike previous designs, this system is insensitive to variations in the input intensity profile and has high throughput efficiency. It consists of two back-to-back Mach–Zehnder interferometers, where the first interferometer converts the linearly polarized input beam into linearly polarized $\sin^2\theta$ and $\cos^2\theta$ intensity distributions by use of novel azimuthally dependent phase plates. The second interferometer combines these beams with high efficiency to create a radially polarized beam. Using this system we have demonstrated a radial-polarization purity of $\approx 92\%$. This system will be used in inverse Čerenkov laser acceleration experiments.

Appendix

The complete analytical description of the radial-polarization converter system is given in this section. A linearly polarized laser beam can be written as

$$E_0 = \exp[i(k\mathbf{r} - \omega t)]f(\mathbf{r})(E_{0x}\hat{\imath} + E_{0y}\hat{\jmath}) \qquad \text{(A1)}$$

where $k = 2\pi/\lambda$; $\hat{\imath}$ and $\hat{\jmath}$ are unit vectors in the x and y directions, respectively; $\mathbf{r} = x\hat{\imath} + y\hat{\jmath}$; $f(\mathbf{r})$ is an arbitrary radial profile; and E_{0x} and E_{0y} are the electric-field components in the x and y directions, respectively. For a linearly polarized beam in the y direction, $E_{0x} = 0$, then

$$E_0 = \exp[i(k\mathbf{r} - \omega t)]f(\mathbf{r})E_{0y}\hat{\jmath}. \qquad \text{(A2)}$$

For the purposes of this analysis we can suppress the radial and temporal dependences of the field and simply write

$$E_0 = E_{0y}\hat{\jmath}. \qquad \text{(A3)}$$

Referring to Fig. 8 for a more detailed schematic of the double interferometer, we see that the input beam is split equally into transmitted and reflected beams E_1 and E_2, respectively,

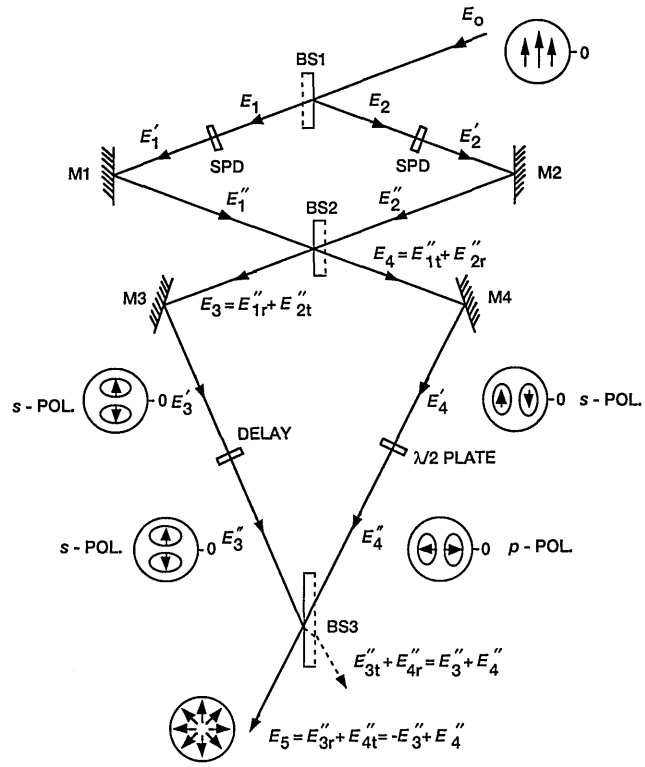

Fig. 8. Detailed schematic of the radial-polarization converter optical system. BS, beam splitter; SPD, spiral-phase-delay plate; M, mirror. The laser beam electric-field directions at various points within the system are also sketched, with $\theta = 0$ defined along the x axis (i.e., 3 o'clock horizontal position).

$$E_1 = \frac{E_{0y}}{\sqrt{2}}\exp(i\Delta\psi_1)\hat{\jmath},$$

$$E_2 = \frac{E_{0y}}{\sqrt{2}}\exp(i\pi)\hat{\jmath} = -\frac{E_{0y}}{\sqrt{2}}\hat{\jmath}, \qquad \text{(A4)}$$

where $\Delta\psi_1$ is an arbitrary phase difference between E_1 and E_2. After passing through the spiral-phase-delay plates, both beams have azimuthal phase terms

$$E_1' = \frac{E_{0y}}{\sqrt{2}}\exp(i\theta)\exp(i\Delta\psi_1)\hat{\jmath},$$

$$E_2' = \frac{-E_{0y}}{\sqrt{2}}\exp(-i\theta)\hat{\jmath}, \qquad \text{(A5)}$$

where θ is the azimuthal angle ($0 < \theta < 2\pi$) measured from the x axis ($+\theta$ for clockwise, $-\theta$ for counterclockwise). Reflecting from mirrors M_1 and M_2 reverses the sign of both beams,

$$E_1'' = -\frac{E_{0y}}{\sqrt{2}}\exp[i(\theta + \Delta\psi_1)\hat{\jmath},$$

$$E_2'' = \frac{E_{0y}}{\sqrt{2}}\exp(-i\theta)\hat{\jmath}. \qquad \text{(A6)}$$

At the second 50/50 beam splitter, both beams generate a pair of reflected and transmitted beams. Accounting for phase shifts, these beams are given by

$$E_{1t}'' = \frac{E_1''}{\sqrt{2}},$$

$$E_{1r}'' = -\frac{E_1''}{\sqrt{2}},$$

$$E_{2t}'' = \frac{E_2''}{\sqrt{2}},$$

$$E_{2r}'' = \frac{E_2''}{\sqrt{2}}, \tag{A7}$$

where the subscripts t and r refer to the transmitted and reflected beams, respectively. Combining these beams yields E_3 and E_4:

$$E_3 = \frac{-E_1'' + E_2''}{\sqrt{2}} = \frac{E_{0y}}{2}\{\exp[i(\theta + \Delta\psi_1)] + \exp(-i\theta)\}\hat{j},$$

$$E_4 = \frac{E_1'' + E_2''}{\sqrt{2}} = \frac{-E_{0y}}{2}\{\exp[i(\theta + \Delta\psi_1)] - \exp(i\theta)\}\hat{j}. \tag{A8}$$

E_3 and E_4 are linearly polarized beams with intensity profiles that vary sinusoidally as a function of θ. The phase shift $\Delta\psi_1$ determines the azimuthal orientation of the beams. For the orientation shown in Fig. 8, $\Delta\psi_1$ can be made equal to π (by, say, adjusting the first interferometer optics), so that $\exp(i\Delta\psi_1) = -1$ and

$$E_3 = \frac{E_{0y}}{2}[-\exp(i\theta) + \exp(-i\theta)]\hat{j} = -iE_{0y}\sin\theta\hat{j},$$

$$E_4 = -\frac{E_{0y}}{2}[-\exp(i\theta) - \exp(-i\theta)]\hat{j} = E_{0y}\cos\theta\hat{j}. \tag{A9}$$

Again these beams change sign after reflecting from M3 and M4

$$E_3' = iE_{0y}\sin\theta\hat{j},$$
$$E_4' = -E_{0y}\cos\theta\hat{j}. \tag{A10}$$

Next the polarization of E_4' is rotated by 90° by use of a half-wave plate. E_3' is sent through a delay plate with a thickness that is the same as that of the half-wave plate to maintain equal path lengths for the two beams to within an arbitrary phase shift $\Delta\psi_2$. The resulting beams are

$$E_3'' = iE_{0y}\exp(i\Delta\psi_2)\sin\theta\hat{j},$$
$$E_4'' = -E_{0y}\cos\theta\hat{\imath}. \tag{A11}$$

The final beam splitter is oriented at Brewster's angle and coated to reflect efficiently s-polarized light (i.e., fields oriented along $\hat{j}$) and to transmit efficiently p-polarized light (i.e., fields oriented along $\hat{\imath}$). Hence the final beam, E_5, consists of the reflected beam, E_3'', and the transmitted beam, E_4'':

$$E_5 = E_{3r}'' + E_{4t}'' = \exp(i\pi)E_3'' + E_4'' = -E_3'' + E_4'', \tag{A12}$$

or, substituting Eq. (A11) into Eq. (A12),

$$E_5 = -E_{0y}(i\sin\theta\exp(i\Delta\psi_2)\hat{j} + \cos\theta\hat{\imath}). \tag{A13}$$

At this point it is more convenient to convert Eq. (A13) to polar coordinates by use of the identities

$$\hat{\imath} = \cos\theta\hat{r} - \sin\theta\hat{\theta},$$
$$\hat{j} = \sin\theta\hat{r} + \cos\theta\hat{\theta}. \tag{A14}$$

Then Eq. (A13) can be rewritten as

$$\begin{aligned} E_5 &= -E_{0y}[i\sin\theta\exp(i\Delta\psi_2)(\sin\theta\hat{r} + \cos\theta\hat{\theta}) \\ &\quad + \cos\theta(\cos\theta\hat{r} - \sin\theta\hat{\theta})], \\ &= -E_{0y}\{\hat{r}[i\sin^2\theta\exp(i\Delta\psi_2) + \cos^2\theta] \\ &\quad + \hat{\theta}[i\sin\theta\cos\theta\exp(i\Delta\psi_2) - \sin\theta\cos\theta]\}. \end{aligned} \tag{A15}$$

Now if we make $\Delta\psi_2 = 3\pi/2$ by adjusting the delay plate, then $\exp(i\Delta\psi_2) = -i$, and Eq. (A15) becomes

$$E_5 = -E_{0y}\hat{r}. \tag{A16}$$

Replacing the radial and temporal dependences in Eq. (A16) that we had ignored earlier and adding a constant phase of $\exp(i\pi) = -1$ gives

$$E_5 = \exp[i(k\mathbf{r} - \omega t)]f(\mathbf{r})E_{0y}\hat{r}. \tag{A17}$$

Comparing Eq. (A17) with the input beam, Eq. (A2), we see that both beams have the same radial profile and amplitude (neglecting small transmission and reflection losses within the interferometer) and that only the direction of polarization has changed. The resulting beam, Eq. (A17), is radially polarized with the electric fields directed along the beam radius.

The authors acknowledge the help of Igor Pogorelsky in analyzing the behavior of the radial polarization converter and thank Igor Pogorelsky and Karl P. Kusche for their assistance during the testing of the radial polarization converter system at the ATF. This work was supported by U.S. Department of Energy contract DE-AC06-83ER40128.

References

1. S. C. Tidwell, D. H. Ford, and W. D. Kimura, "Generating radially polarized beams interferometrically," Appl. Opt. **29,** 2234–2239 (1990).
2. W. D. Kimura, R. D. Romea, S. C. Tidwell, and D. H. Ford, "Progress on inverse Čerenkov laser accelerator experiment," in *Advanced Accelerator Concepts,* AIP Conf. Proc. **193,** 203–216 (1989).
3. R. D. Romea and W. D. Kimura, "Modeling of inverse Čerenkov

laser acceleration with axicon laser beam focusing," Phys. Rev. D **42,** 1807–1818 (1990).
4. T. V. Higgins, "Spiral waveplate design produces radially polarized laser light," Laser Focus World **28**(4), 18–20 (1992).
5. J. R. Fontana and R. H. Pantell, "A high-energy laser accelerator for electrons using the inverse Cherenkov effect," J. Appl. Phys. **54,** 4285–4288 (1983).
6. S. C. Tidwell, D. H. Ford, and W. D. Kimura, "Transporting and focusing radially polarized laser beams," Opt. Eng. **31,** 1527–1531 (1992).